Ore Geology Reviews 148 (2022) 105034

Contents lists available at ScienceDirect

Ore Geology Reviews

journal homepage: www.elsevier.com/locate/oregeorev

Late mesozoic magmatism in the Gucheng district: Implications for REE metallogenesis in South China

Yuzhou Feng [a,b], Bing Xiao [a,b,*], Gaobin Chu [a,b], Shasha Li [a,b,c], Jun Wang [a,b,c], Zhenquan Wen [a,b,c]

[a] Guangzhou Institute of Geochemistry, Chinese Academy of Sciences, Guangzhou 510640, China
[b] CAS Center for Excellence in Deep Earth Science, Guangzhou, 510640, China
[c] Geology Bureau for Nonferrous Metals of Guangdong Province, Guangzhou, 510640, China

ARTICLE INFO

Keywords:
Late Cretaceous granites
Magmatism
Regolith-hosted REE deposit
Gucheng district
South China

ABSTRACT

Regolith-hosted rare earth element (REE) deposits are common in South China. The newly-discovered Gucheng REE deposit in the western part of Guangdong Province, is characterized by HREE enrichment (with ∑HREE oxides of 55%). Three types of granites have been identified in the Gucheng ore district, a REE-fertile coarse-grained biotite granite (CGBG), a weakly REE-fertile fine-grained biotite granite (FGBG) and the barren medium-grained biotite granite (MGBG). New LA-ICP-MS zircon U-Pb dating reveals that the MGBG (107.7 ± 0.4 Ma), CGBG (103.2 ± 0.6 Ma) and the FGBG (98.9 ± 0.7 Ma) were all formed in the Late Cretaceous.

Mineralogical and geochemical data indicate that the CGBG is an unfractionated I-type granite, whereas the FGBG and MGBG are fractionated I-type granites. The CGBG and FGBG have $(^{87}Sr/^{86}Sr)_i$ and εNd(t) ranging from 0.7121 to 0.7140 and −8.6 to −8.0, and 0.7125 to 0.7131 and −8.2, respectively. The source of these granites was mainly composed of two end-members: one having 90% Paleoproterozoic basement and another 10% enriched mantle metasomatized by subduction-related melts. The barren MGBG is also derived from partial melting of a Paleoproterozoic source with a minor contribution of enriched mantle. The involvement of enriched mantle can provide REE into the magmas, which plays an important role in REE enrichment. Geochemical data show that allanite have been crystallized during magma evolution process of all the three types of granites. However, no allanite has been discovered in the MGBG, and the FGBG contains lower abundance of allanite than that of the CGBG, which is due to different degrees of fractionation. The crystallization and separation of allanite has greatly affected the LREE of the three types of granites, which further influences their potential for LREE mineralization. Lower K/Rb and Nb/Ta ratios of the CGBG, FGBG and MGBG indicate that these three types of granites were affected by hydrothermal events after their crystallization. Zircon geochemical data show that the MGBG was formed in a lower oxygen fugacity environment than the CGBG and FGBG. Above all, involvement of enriched mantle, a relatively high oxygen fugacity, crystallization and separation of allanite as well as involvement of hydrothermal events after magmatic crystallization are important factors controlling REE mineralization at Gucheng, of which the hydrothermal events may play the most important role.

1. Introduction

The rare earth elements (REEs), comprising the lanthanide group of elements from lanthanum (La) to lutetium (Lu) plus yttrium (Y) and scandium (Sc), are important in a variety of advanced technological applications. Currently, almost 35% of the REE production all around the world comes from regolith-hosted REE deposits clustered in South China, which are also referred to as "ion-adsorption REE deposits" (Sanematsu and Watanabe, 2016; Jowitt et al., 2017; Li et al., 2017). >170 regolith-hosted REE deposits have been discovered in South China (Xie et al., 2016; Li et al., 2017), with a total of >1.3 Mt rare earth oxides (REOs) resources (Xie et al., 2016). Most of these regolith-hosted REE deposits can be classified into highly HREE-enriched (with ∑HREE oxides >70% of the total REE resources) and highly LREE-enriched (with ∑LREE oxides >70% of the total REE resources) (Li et al., 2017). It is now accepted that most of regolith-hosted REE deposits are

* Corresponding author at: Guangzhou Institute of Geochemistry, Chinese Academy of Sciences, Guangzhou 510640, China.
E-mail address: xiaobing7960@126.com (B. Xiao).

https://doi.org/10.1016/j.oregeorev.2022.105034
Received 23 June 2022; Received in revised form 16 July 2022; Accepted 18 July 2022
Available online 22 July 2022

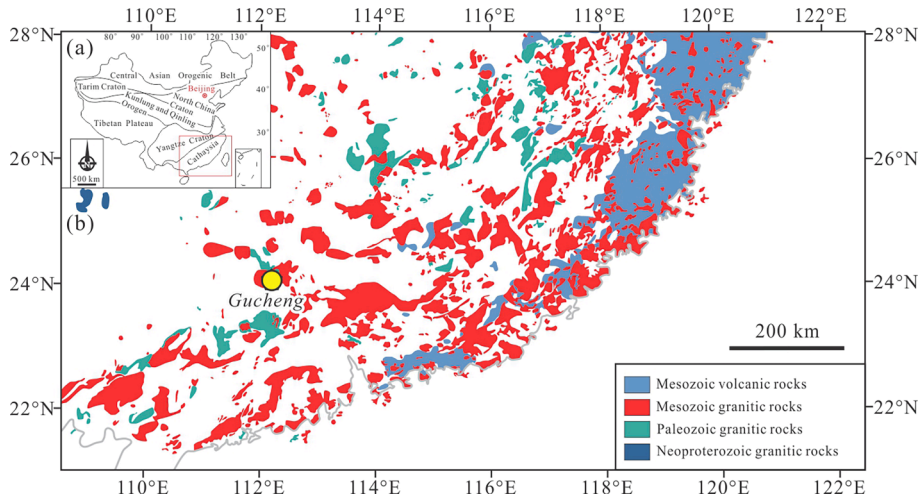

Fig. 1. (a) Sketched map showing the location of the South China; (b) The distribution of granites and volcanic rocks in South China (after Li et al., 2019). The location of the Gucheng deposit is marked with a yellow circle.

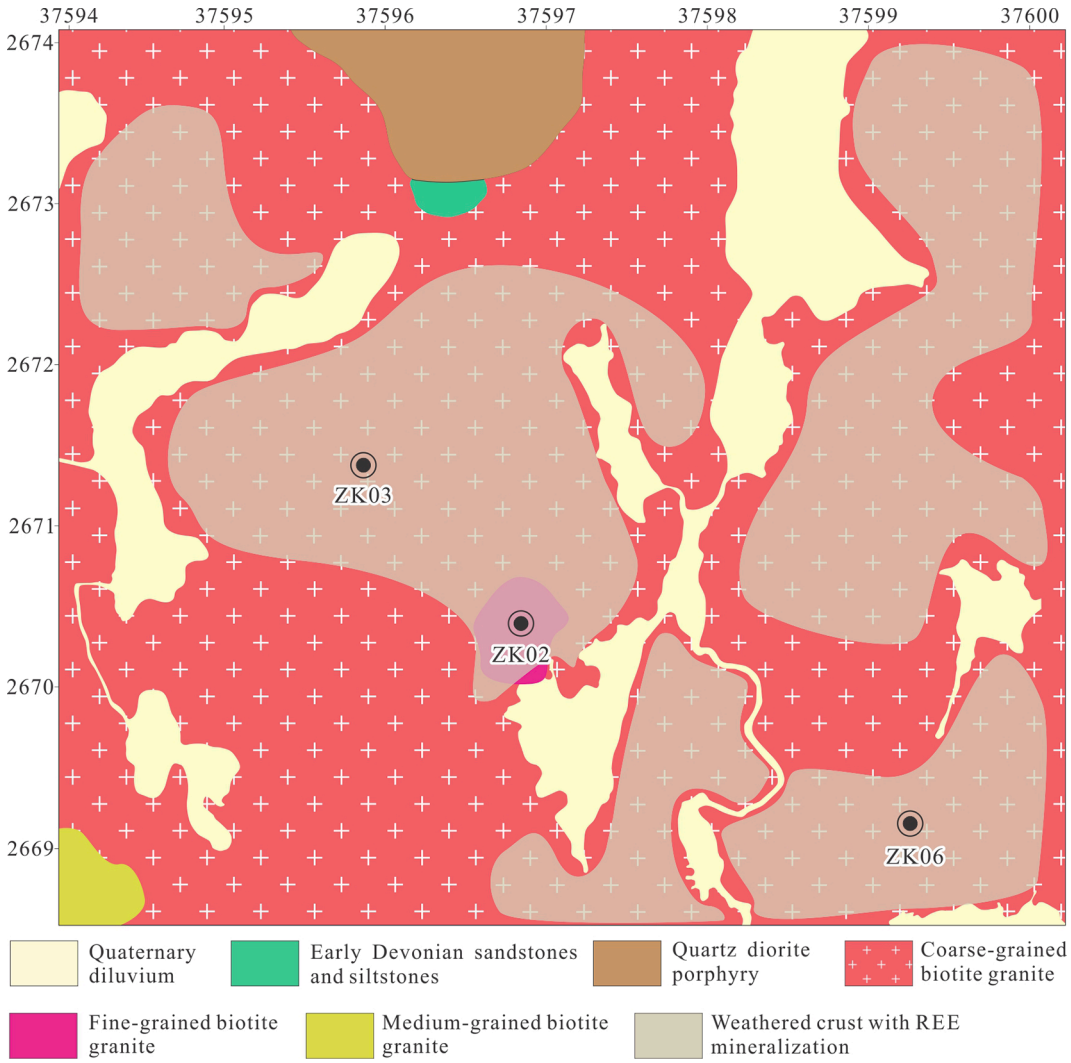

Fig. 2. Geologic map of the Gucheng ore district, showing locations of drill holes of ZK02, ZK03 and ZK06.

hosted within the weathered crusts of granites and consequently the parental granite may have influenced the ore formation (Bao and Zhao, 2003; Murakami and Ishihara, 2008; Li et al., 2017, 2019, 2020). Granites are widespread in South China, whilst REE mineralization just occur in the weathered curst of some granites, and some weathered crusts of granites do not host REE mineralization. Detailed

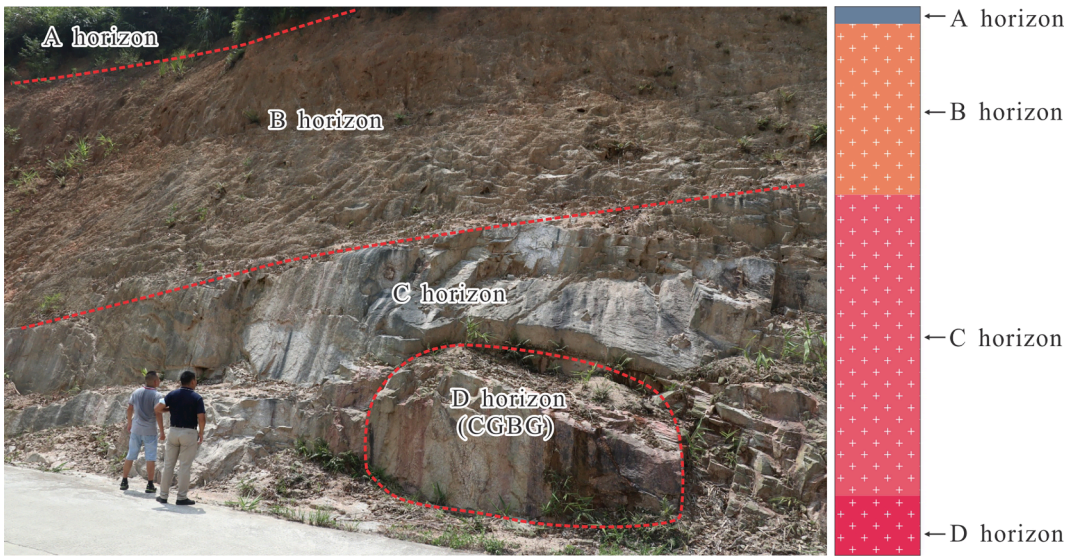

Fig. 3. A cross-section showing A, B, C and D horizons and a schematic soil profile at Gucheng.

investigations of the geochemical and petrological relationships between *syn*-mineralization granites, barren granites and the presence of REE mineralization are required to enhance our understanding of this type of deposit.

The Gucheng deposit is a newly discovered REE deposit in South China. Mineral exploration is ongoing in the Gucheng district, and it is HREE-enriched with ∑HREE oxides of about 55%. Although the exploration results appear promising, resource estimates have yet to be publicly disclosed. At Gucheng, three types of granites have been discovered, a REE-fertile coarse-grained biotite granite (CGBG), a weakly REE-fertile fine-grained biotite granite (FGBG) and the medium-grained biotite granite (MGBG) that has no obvious association with REE mineralization. We studied the geological, ages and geochemical features of the three types of granites in this study to investigate the petrogenesis of three types of granites, and the geochemical and petrological relationships between *syn*-mineralization granites and barren granites, as well as to provide information and new insights on the genesis of the Gucheng deposit.

2. Geological setting

The Gucheng deposit is located at the southwest part of South China (Fig. 1), a major polymetallic mineralization region. Large volumes of granitic rocks were emplaced during the Late Permian, Triassic, Jurassic and Cretaceous in this region. These granites intruded into Proterozoic to Cambrian mudstones, sandstones, and shales, and Devonian to Early Permian carbonate rocks (Li et al., 2017; Zhao et al., 2017). The REE mineralization is temporally and spatially associated with granitic rocks that formed during the Middle Jurassic to Late Cretaceous. Large numbers of regolith-hosted REE deposits have been discovered in the region, such as the Zudong, Zhaibeiding, Bachi, Dabu and Guposhan (Li et al., 2017, 2019).

The local stratigraphy at Gucheng is composed of Early Devonian and Quaternary units. The Early Devonian rocks, locally exposed in the north, are dominated by sandstones and siltstones. The Quaternary rocks are widely exposed at Gucheng, and mainly consist of diluvium (Fig. 2). The REE deposit was formed by weathering of the Gucheng pluton, a granitic stock exposed over an area of 30 km^2. At Gucheng, igneous rocks are extensively developed, including the CGBG, FGBG, MGBG and quartz diorite porphyry. The CGBG is widely exposed in the Gucheng deposit with outcrops over 20 km^2, whereas the FGBG is less common but is found in several drill holes. The MGBG and quartz diorite porphyry are found only in southwestern and northern parts of the Gucheng deposit, respectively (Fig. 2).

The CGBG, FGBG and MGBG have all been intensely weathered, but the REE mineralization occurs only in the weathered crust of the CGBG and FGBG, which has been reported by the Geology Bureau for Nonferrous Metals of Guangdong Province. Soil profiles at the Gucheng deposit vary from a few meters to >30 m thick. The soil–bedrock profile can be divided into four horizons, namely the A horizon, a humic soil zone; the B horizon composed of a completely weathered zone with enriched clay minerals; the C horizon composed of incompletely weathered bedrock and the D horizon of fresh bedrock (Fig. 3). The economic orebodies are hosted mainly within the B horizon and less commonly within the C horizon.

3. Petrography of the Gucheng granites

The contact relationships and petrographic characteristic of the three types of granite at Gucheng are presented in Fig. 4.

3.1. Coarse-grained biotite granite (CGBG)

The CGBG has a pink mottled appearance (Fig. 4a-b), and consists mainly of K-feldspar (~20 vol%), plagioclase (~30 vol%), quartz (~32 vol%), biotite (~8 vol%) and hornblende (<5 vol%) (Fig. 4c-e). Accessory minerals (<5 vol%) include allanite, titanite, apatite, zircon and Fe-Ti oxides (Fig. 4c–e). Some allanite and titanite grains have been partially replaced by hydrothermal fluid and altered into synchysite and gadolinite, respectively (Fig. 4d–e). As the major ore-causative granite reported by the Geology Bureau for Nonferrous Metals of Guangdong Province, the near surface occurrences of the CGBG are intensely altered and weathered. As a result, in the B horizon the original granitic texture has been completely destroyed. In the C horizon, the original texture of the parent granite is largely preserved (Fig. 4b), but the K-feldspar and plagioclase have been partially altered to clay minerals, and the biotite and hornblende have been partially altered to chlorite.

3.2. Fine-grained biotite granite porphyry (FGBG)

The FGBG intruded into the CGBG with sharp intrusive contacts (Fig. 4f). The rocks are grayish-white (Fig. 4g), and contain mainly K-feldspar (~20 vol%), plagioclase (~32 vol%), quartz (~35 vol%) and biotite (~8 vol%), with grain sizes <1 mm (Fig. 4h-i). Accessory minerals (<5 vol%) include allanite, apatite, zircon and Fe-Ti oxides (Fig. 4h-i). The abundance of allanite and apatite in the FGBG is lower

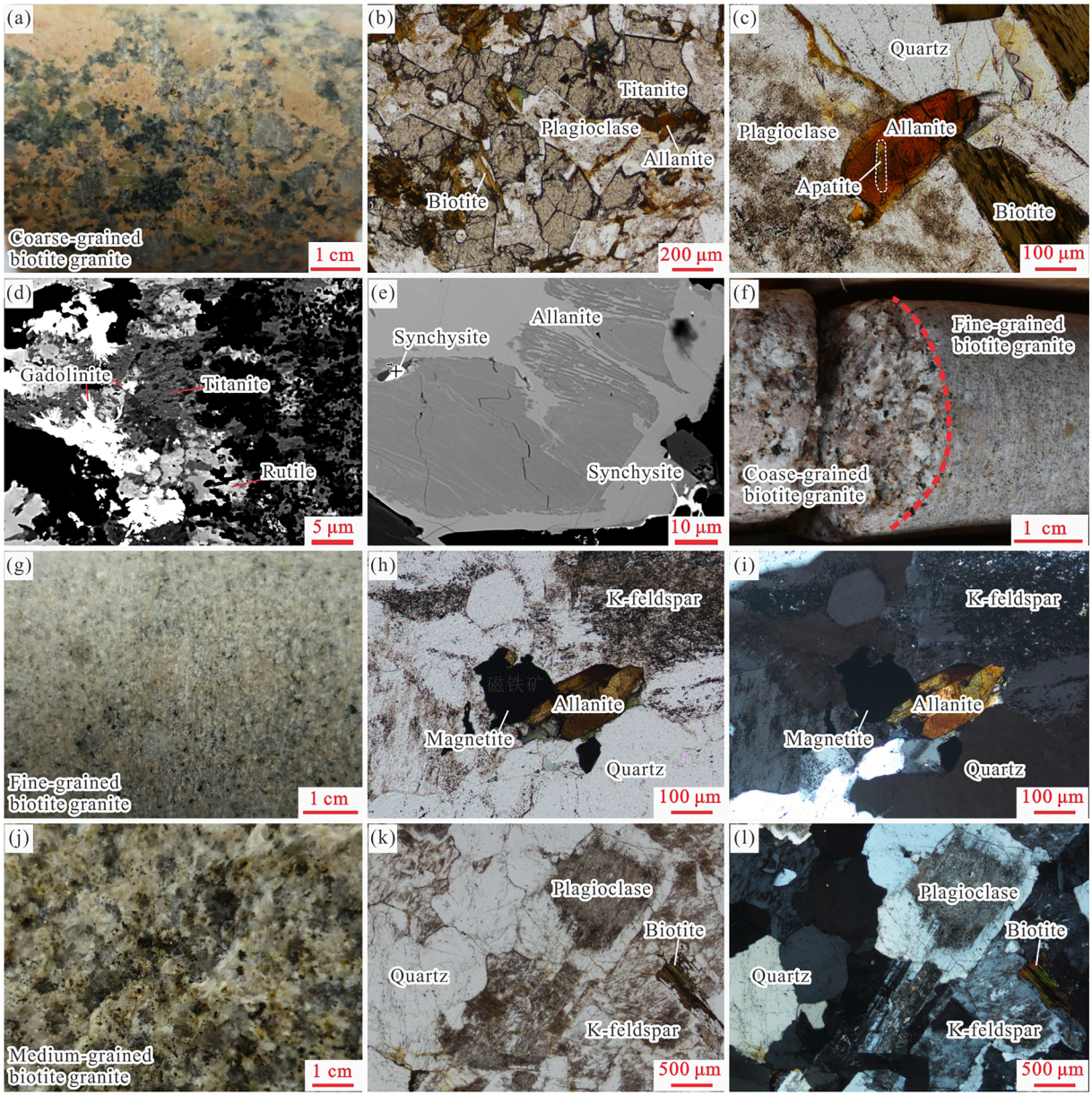

Fig. 4. Photomicrographs showing the characteristics of the coarse-grained biotite granite (CGBG), fine-grained biotite granite (FGBG) and medium-grained biotite granite (MGBG). (a) A hand sample of the fresh CGBG with pink mottled appearance and coarse-grained minerals; (b) A hand sample of the weathered CGBG with the minerals being intensely altered; (c-d) Micrographs showing minerals of plagioclase, quartz, biotite, allanite, apatite and titanite in the CGBG; (e) A back-scattered image showing that the synchysite occurred in the cave or along the margin of allanite; (f) Sharp intrusive contact between the CGBG and FGBG; (g) A hand sample of the fresh FGBG with grey appearance and fine-grained minerals; (h-i) Micrographs showing minerals of K-feldspar, quartz, allanite and magnetite in FGBG; (j) A hand sample of the fresh MGBG with grey appearance and medium-grained minerals; (k-l) Micrographs showing minerals of biotite, plagioclase, K-feldspar and quartz in MGBG.

than that in the CGBG. The FGBG rocks on the surface have been intensely weathered, with weak mineralization developed in the completely weathered zone (B horizon).

3.3. Medium-grained biotite granite (MGBG)

The MGBG is rarely exposed in southwest part of the Gucheng deposit, but no obvious contact relationships with the CGBG and FGBG were observed. These rocks are characterized by intermediate grains, are grey in color, and are composed of mainly K-feldspar (~25 vol%), plagioclase (~32 vol%) and quartz (~35 vol%) as well as minor biotite (~3 vol%) (Fig. 4k-l). Accessory minerals (<5 vol%) include apatite and zircon. The abundance of apatite is lower than in the CGBG and FGBG. The granites have been intensely weathered, but no mineralization has been identified in the weathered profile, which has been analyzed by the Geology Bureau for Nonferrous Metals of Guangdong Province.

4. Sampling and methods

In this study, the least altered samples were collected from the CGBG, FGBG and MGBG, mostly from the drill core but with a small number from outcrops. Three samples from each of the fresh CGBG (ZK03-1), FGBG (ZK02-1) and MGBG (GC03) were chosen for zircon U-Pb dating. Four fresh CGBG samples from drill cores of ZK03 and ZK06 and three fresh FGBG samples from drill core of ZK02 and three fresh MGBG samples from outcrops were chosen for major and trace element analyses. Four fresh CGBG samples from drill cores of ZK03 and ZK03, three fresh FGBG samples from the drill core of ZK02 and two fresh MGBG

Table 1
Sample location and features of the main magmatic rocks at Gucheng.

Sample No.	Drilling or outcrop	Lithology	Location		
			Easting	Northing	Depth (m)
ZK03-3	ZK03	Coarse-grained granite	37595.8	2671.4	51.0
ZK03-6	ZK03	Coarse-grained granite	37595.8	2671.4	59.0
ZK06-6	ZK06	Coarse-grained granite	37599.2	2669.1	29.0
ZK06-8	ZK06	Coarse-grained granite	37599.2	2669.1	33.0
ZK02-1	ZK02	Fine-grained granite	37596.9	2670.2	16.0
ZK02-3	ZK02	Fine-grained granite	37596.9	2670.2	18.0
ZK02-4	ZK02	Fine-grained granite	37596.9	2670.2	22.0
GC01	Outcrop	Medium-grained granite	37594.1	2668.5	148.0
GC02	Outcrop	Medium-grained granite	37594.1	2668.4	150.6
GC03	Outcrop	Medium-grained granite	37594.1	2668.4	150.6

samples from outcrops were collected for Sr-Nd isotopic analyses. Sample locations and lithologies are presented in Table 1.

4.1. Zircon U-Pb dating

Zircon grains were separated from samples using conventional heavy liquids and magnetic separation techniques, and handpicked under a binocular microscope. Zircon CL images were obtained using a TESCAN MIRA3 field-emission scanning electron microprobe (FE-SEM) at the Testing Center, Tuoyan Analytical Technology Co. Ltd. (Guangzhou, China). Working conditions of the CL imaging have been described in detail by Zhang et al. (2019). Zircon U-Pb dating of was conducted by LA-ICP-MS at the Guangzhou Tuoyan Analytical Technology Co., Ltd., Guanzhou, China. Laser sampling was performed using a NWR 193 laser ablation system. An iCAP RQ ICP-MS instrument was used to acquire ion-signal intensities. Helium was used as a carrier gas. Argon was used as the make-up gas and mixed with the carrier gas via a Y-connector before entering the ICP. The spot size and frequency of the laser were set to 30 μm and 8 Hz, respectively, in this study. The energy was 5 J/cm^2. Zircon 91,500 (Wiedenbeck et al., 1995) and glass NIST610 (Reed, 1992) were used as external standards for U-Pb dating and trace element calibration, respectively. Each analysis incorporated a background acquisition of approximately 30 s followed by 40 s of data acquisition from the sample. The Excel-based software ICPMSDataCal was used to perform off-line selection and integration of the background and analysis signals, time-drift correction and quantitative calibration for U-Pb dating and trace element analysis (Liu et al., 2008). The results of zircon U-Pb dating of three types of granites are listed in Supplementary Appendix 1 and illustrated in Fig. 5.

4.2. Whole-rock major and trace element compositions

Whole-rock major and trace element analyses were conducted at the Sample Solution Co. Ltd. (Wuhan, China). Major oxide contents were determined by XRF spectrometry. Fused glass disks with Lithium Borate were used and the analytical precisions were better than ±0.1%, based on repeated analyses of the standards GSR-2 and GSR-3. Trace element concentrations were determined by ICP-MS. Analyses of USGS rocks standards (BCR-2, BHVO-1 and AGV-1) reveal that the precision and accuracy were better than ±5% for the trace elements studied. Detailed analytical methods and procedures are reported in Zhang et al. (2019). Whole-rock geochemical data for the four CGBG samples, three FGBG samples and three MGBG samples are listed in Supplementary Appendix 2.

4.3. Whole-rock Sr-Nd isotopic analyses

Sr and Nd isotopic analyses were undertaken with a Micromass ISOprobe MC-ICP-MS at the Sample Solution Co. Ltd. (Wuhan, China), using the analytical methods described by Zhang and Hu (2020). Strontium was separated using cation columns, and Nd fractions were further separated using HDEHP-coated Kef columns. Measured $^{87}Sr/^{86}Sr$ and $^{143}Nd/^{144}Nd$ ratios were normalized to $^{86}Sr/^{88}Sr = 0.1194$ and $^{146}Nd/^{144}Nd = 0.7219$, respectively. The reported $^{87}Sr/^{86}Sr$ and $^{143}Nd/^{144}Nd$ ratios were adjusted to the NBS SRM 987 standard of $^{143}Nd/^{144}Nd = 0.512115$. The Sr-Nd isotopic compositions of the CGBG, FGBG and MGBG are shown in Table 2.

5. Results

5.1. Zircon U-Pb ages

At Gucheng, all the zircons of the three types of granites analyzed are colorless to light gray in CL images, euhedral to subhedral, and show fine-scale oscillatory igneous growth zones. Meanwhile, the zircon grains of the CGBG, FGBG and MGBG have high Th/U ratios ranging from 0.45 to 0.99, 0.34 to 1.32 and 0.15 to 1.32, respectively, indicating an igneous origin (Koschek, 1993).

Coarse-grained biotite granite: Twenty zircon grains yielded $^{206}Pb/^{238}U$ ages ranging from 97.2 ± 2.0 to 107.3 ± 1.1 Ma, with the concordia age of 103.2 ± 0.6 Ma (MSWD = 1.5; Fig. 5a) and a weighted mean age of 103.2 ± 0.3 Ma (MSWD = 3.8; Fig. 5b), indicating that the CGBG granite was formed in the Late Cretaceous.

Fine-grained granite: The $^{206}Pb/^{238}U$ ages of twenty analytical spots ranged from 95.3 ± 1.6 to 101.6 ± 1.3 Ma, yielding a concordia age of 98.9 ± 0.7 Ma (MSWD = 1.1; Fig. 5c) and weighted mean age of 98.7 ± 0.3 Ma (MSWD = 1.5; Fig. 5d), indicating that the FGBG granite was formed in the Late Cretaceous.

Medium-grained granite: The $^{206}Pb/^{238}U$ ages of twenty analytical spots range from 101.0 ± 1.6 to 113.2 ± 2.5 Ma, yielding a concordia age of 107.7 ± 0.4 Ma (MSWD = 3.6; Fig. 5e) and weighted mean age of 107.6 ± 0.3 Ma (MSWD = 4.0; Fig. 5f), indicating that the MGBG was formed in the Late Cretaceous.

5.2. Major and trace element compositions

Coarse-grained biotite granite: The samples have SiO_2 = 70.94–75.41 wt% (avg. 73.07 wt%), Total Fe_2O_{3T} = 2.41–3.08 wt% (avg. 2.68 wt%), ($Na_2O + K_2O$) = 6.76–8.86 wt% (avg. 8.66 wt%), (K_2O/ Na_2O) = 1.09–1.82 (avg. 1.41) and a differentiation index (DI) of 85.50–87.80 (avg. 86.57). In the Q' vs. ANOR diagram (Fig. 6a; Irvine and Baragar, 1971) and K_2O vs. SiO_2 diagram (Fig. 6b; Peccerillo and Taylor, 1976), the CGBG samples were plot in the monzogranite and high-K calc-alkaline and shoshonite fields. Their A/CNK values (0.98–1.00) suggest they are metaluminous (Fig. 6c; Maniar and Piccoli, 1989). The CGBG is enriched in LREE [$(La/Yb)_N$ = 4.00–10.65] as well as Th (35.6–50.6 ppm), U (10.9–15.9 ppm), K (29225–47406 ppm), Pb (28.5–40.8 ppm), Zr (146–216 ppm) and Hf (4.75–6.30 ppm), but depleted in HREE, Ba (162–643 ppm), Nb (17.4–25.3 ppm), Sr (98.3–132 ppm), P (410–472 ppm) and Ti (1914–2466 ppm) (Fig. 7). The rocks have Rb/Sr ratios of 2.02–2.57, Sr/Y of 2.45–4.60, Nb/Ta ratios of 5.29–13.39 and 104 × Ga/Al values of 2.36–2.59, with negative Eu anomalies (δEu = 0.31–0.61).

Fine-grained biotite granite: The samples have SiO_2 = 76.02–77.32 wt % (avg. 76.64 wt%), Total Fe_2O_{3T} = 1.20–1.53 wt% (avg. 1.37 wt%), ($Na_2O + K_2O$) = 8.08–8.30 wt% (avg. 8.22 wt%), (K_2O/ Na_2O) = 1.38–1.79 (avg. 1.56) and DI of 92.74–94.26 (avg. 93.46). The rocks are syenogranite (Fig. 6a) and (high-K) calc-alkaline (Fig. 6b). Their A/CNK

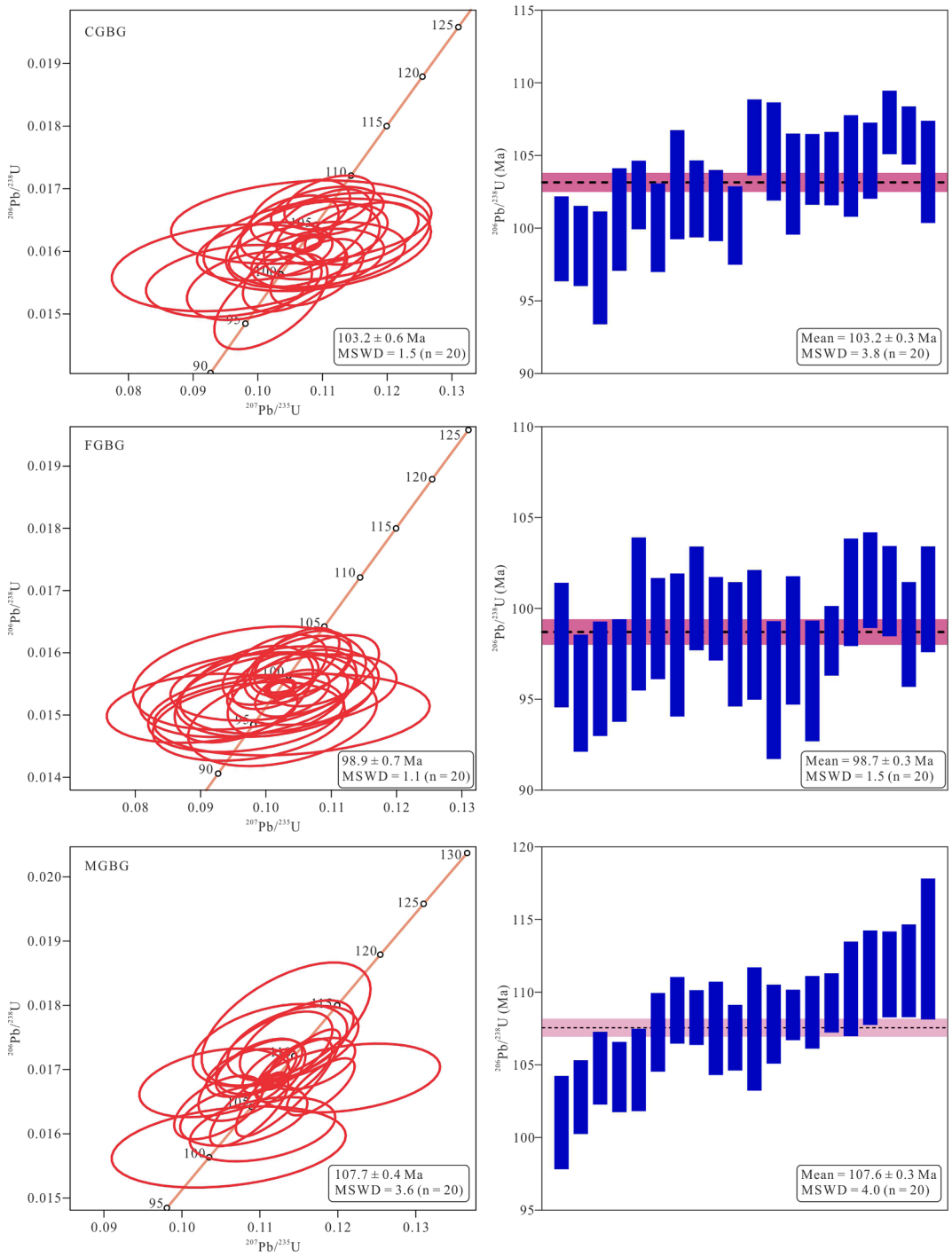

Fig. 5. Concordia diagrams and weighted mean zircon U-Pb ages for the CGBG, FGBG and MGBG granites.

values vary from 1.01 to 1.02, suggesting that the fine-grained granite is weakly peraluminous (Fig. 6c). Similar to the CGBG, the FGBG is also enriched in LREE [$(La/Yb)_N$ = 3.09–4.38], Th (44.8–47.6 ppm), U (18.5–22.5 ppm), K (38909–44194 ppm), Pb (40.7–45.1 ppm), Zr (110–153 ppm) and Hf (4.52–5.92 ppm), and depleted in HREE, Ba (58.5–289 ppm), Nb (18.9–26.5 ppm), Sr (26.4–54.1 ppm), P (96.1–165.9 ppm) and Ti (684–924 ppm) (Fig. 7). The rocks have more intensely negative Eu anomaly (δEu = 0.21–0.36). Meanwhile, the rocks have similar 10000 × Ga/Al values (2.48–2.57) as the CGBG, but have higher Rb/Sr ratios (6.97–15.25) as well as lower Sr/Y (0.75–1.62) and Nb/Ta ratios (4.93–5.93).

Medium-grained biotite granite: The samples have SiO_2 = 77.15–77.75 wt% (avg. 77.38 wt%), Fe_2O_{3T} = 1.04–1.14 wt% (avg. 1.07 wt%), (Na_2O + K_2O) = 7.97–8.18 wt% (avg. 8.07 wt%), (K_2O/ Na_2O) = 1.23–1.33 (avg. 1.27) and DI of 94.98–95.17 (avg. 95.06). The MGBG samples plot in the syenogranite field (Fig. 6a). These rocks are (high-K) calc-alkaline (Fig. 6b) and weakly peraluminous (Fig. 6c) with A/CNK values varying from 1.03 to 1.04. The rocks are characterized by a weaker enrichment of LREE [$(La/Yb)_N$ = 1.51–1.76] than the CGBG and FGBG, and have relatively high Th (41.8–44.2 ppm), U (17.2–19.3 ppm), K (36909–37805 ppm), Pb (55.9–57.7 ppm), Zr (97.5–103 ppm) and Hf (4.79–5.21 ppm), and low Ba (21.1–23.0 ppm), Nb (39.7–51.7 ppm), Sr (10.3–11.5 ppm), P (39.3–43.7 ppm) and Ti (330–438 ppm) (Fig. 7). The MFBG has the largest negative Eu anomalies (δEu = 0.06–0.07), Rb/Sr

Table 2
Whole rock Sr-Nd isotopic compositions of the granites at Gucheng.

Sample No.	Lithology	$^{87}Sr/^{86}Sr$	2SE	Rb	Sr	Isr	$^{143}Nd/^{144}Nd$	2SE	Sm	Nd	$^{147}Sm/^{144}Nd$	εNd (t)	T_{2DM} (Ma)
ZK03-3	Coarse-grained granite	0.722536	0.000007	248	123	0.713970	0.512164	0.000005	7.53	30.20	0.15	−8.6	1605
ZK03-6	Coarse-grained granite	0.722848	0.000008	248	98.3	0.712129	0.512163	0.000004	6.71	36.60	0.11	−8.1	1564
ZK06-6	Coarse-grained granite	0.724711	0.000007	337	132	0.713862	0.512154	0.000004	5.26	26.20	0.12	−8.5	1590
ZK06-8	Coarse-grained granite	0.723118	0.000006	289	112	0.712154	0.512169	0.000005	5.77	31.30	0.11	−8.0	1556
ZK02-1	Fine-grained granite	0.753282	0.000008	352	35.7	0.713100	0.512179	0.000010	4.89	21.10	0.14	−8.2	1569
ZK02-3	Fine-grained granite	0.774822	0.000008	403	26.4	0.712477	0.512173	0.000006	4.63	22.10	0.13	−8.2	1565
GC01	Medium-grained granite						0.512244	0.000004	6.33	20.10	0.19	−7.6	
GC02	Medium-grained granite						0.512232	0.000004	5.98	20.80	0.17	−7.6	

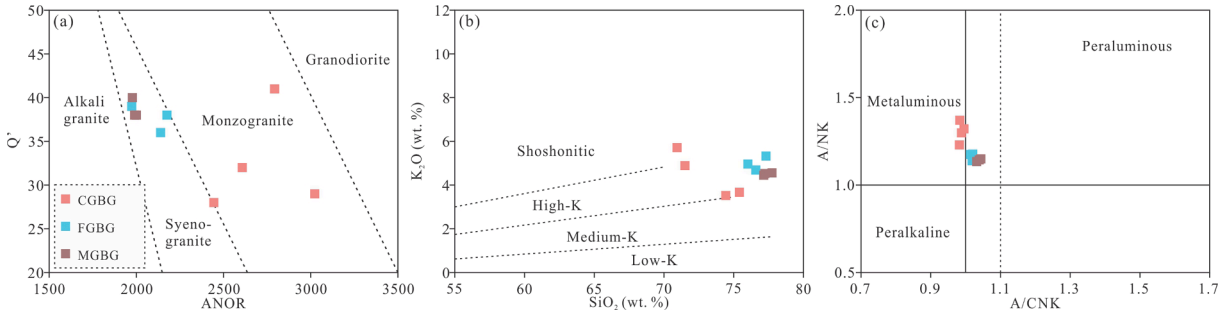

Fig. 6. Plots of Q' vs. ANOR (Streckeisen and Le Maitre, 1979) (a) SiO_2 vs. K_2O (b, Irvine and Baragar, 1971) and A/CNK vs. A/NK (c, Peccerillo and Taylor, 1976) for the CGBG, FGBG and MGBG granites. Q' = Q/(Q + Or + Ab + An) * 100; ANOR = An/(Or + An) * 100.

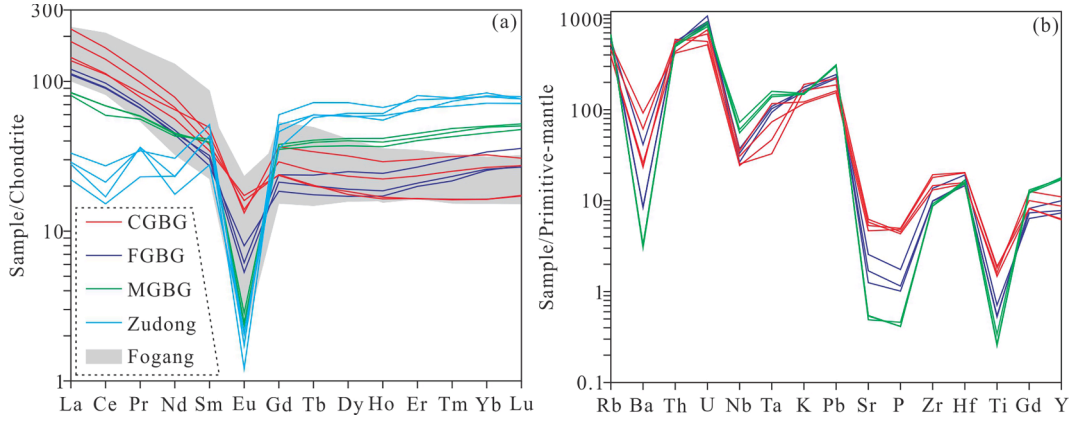

Fig. 7. Chondrite-normalized REE pattern (a, normalizing values from Sun and McDonough, 1989) and primitive mantle-normalized trace elements (b, normalizing values from Sun and McDonough, 1989) for the CGBG, FGBG and MGBG granites (data of Fogang granites are from Bao and Zhao, 2003; data of Zudong granites are from Huang et al., 1989).

ratios (39.3–43.7), and 10^4 × Ga/Al values (2.89–3.09).

5.3. Whole-rock Sr-Nd isotope data

In our study, the initial $^{87}Sr/^{86}Sr$ ratios of the three types of granites were calculated on the basis of their corresponding weighted mean ages. The CGBG samples have $(^{87}Sr/^{86}Sr)_i$ ratios, εNd(t) values and T_{2DM} of 0.7121 to 0.7140, −8.6 to −8.0 and 1556 to 1605 Ma, respectively. The FGBG samples have $(^{87}Sr/^{86}Sr)_i$, εNd(t) values and two-stage Nd model ages (T_{2DM}) of 0.7125 to 0.7131, −8.2 and 1565 to 1569 Ma, respectively, which are similar to those of the CGBG. The MGBG samples have relatively high Rb/Sr ratios (36.11–41.49), meaning that the initial $^{87}Sr/^{86}Sr$ ratios could not be calculated (Jahn et al., 2000). The εNd(t) values T_{2DM} and of two samples are calculated both to be −7.6 and 1524 to 1525 Ma.

6. Discussion

6.1. Petrogenesis of the Late Cretaceous magmatism at Gucheng

In our study, samples of the three types of granites all have low LOI (0.22–0.79), suggesting that the compositions of the three types of granites have not been greatly mobilized (Asadi et al., 2014) and are valid to reveal their petrogenesis. Most granitoids in South China were

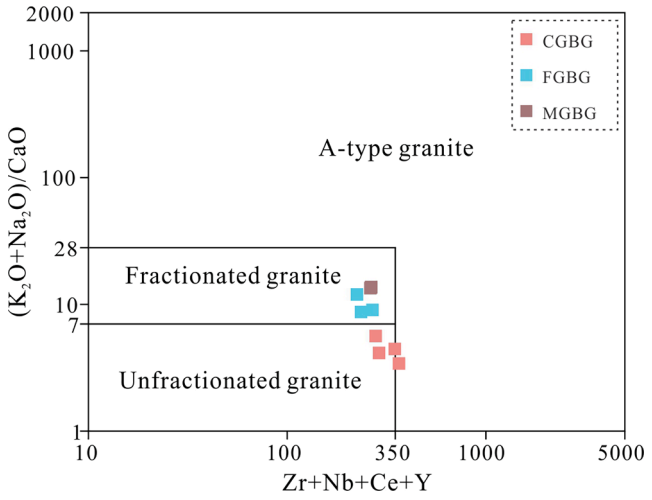

Fig. 8. ($K_2O + Na_2O$)/CaO vs. (Zr + Nb + Ce + Y) classification diagrams of Whalen et al. (1996). The CGBG granites are typical of I-type, and the FGBG and MGBG granites are fractionated I-type.

emplaced during the Mesozoic, with I-, S- and A-types all having been recognized (Li et al., 2007a). At Gucheng, the CGBG is likely I-type granite, given the presence of amphibole and titanite. The CGBG has A/CNK values below 1.1, in contrast to the felsic S-type granites that are usually strongly peraluminous with A/CNK values much higher than 1.1 (Chappell, 1999). As previous studies suggested, the I-type granites have P_2O_5 contents below 0.14%, because apatite reaches saturation in metaluminous and mildly peraluminous magmas (A/CNK < 1.1), but is highly soluble in strongly peraluminous melts (Wolf and London, 1994; Chappell, 1999). Therefore, P_2O_5 contents is also an important criterion for distinguishing I-type granites from S-type granites. At Gucheng, the CGBG has P_2O_5 contents of 0.09 to 0.11 wt%, further indicating that the CGBG is I-type granite. The FGBG and MGBG are also high K calc-alkaline and have A/CNK values below 1.1 and lower P_2O_5 contents (<0.14 wt%; Wolf and London, 1994), indicating that these rocks are also I-type granites. On the other hand, the CGBG has low (K_2O + Na_2O)/CaO (3.42–5.63) and Zr + Nb + Y + Ce (279–365 ppm) values, falling into the unfractionated granite field (Fig. 8), indicating that the CGBG are unfractionated I-type. However, the FGBF and MGBG are plotted into the fractionated granite field, indicating that these two types of granites are fractionated I-type.

As previous studies suggested, the high-K calc-alkaline I-type granitoids can be produced by advanced assimilation fractional crystallization of mantle-derived basaltic magmas (Singer et al., 1992; Soesoo, 2000; Clemens et al., 2011) or by partial melting of infracrustal mafic to intermediate igneous sources in the lower continental crust (Chappell et al., 1987; Chappell, 1999; Kemp et al., 2006, 2007; Hawkesworth and Kemp, 2006). The former process can be excluded due to that (1) the mafic or intermediate rocks are not discovered in the Gucheng district and (2) the mafic microgranular enclaves are absent in all the three types of granites. Therefore, the three types of granites at Gucheng are derived from infracrustal igneous sources. The three types of granites at Gucheng have T_{2DM} values of 1524 to 1605 Ma, indicating that they are derived from the Meso- or Paleoproterozoic rocks. The Paleoproterozoic (1.8–2.2 Ga; Bao and Zhao, 2003) is an important timing of crustal growth in South China, and the Paleoproterozoic rocks have been proved to be source of the most Mesozoic granitic rocks in South China (Li et al., 2007a). However, the Mesoproterozoic rocks have not been reported in South China (Chen et al., 1999; Bao and Zhao, 2003). Therefore, the three types of granites at Gucheng are likely derived from partial melting of the Paleoproterozoic rocks. On the other hand, the εNd (t) values of the CGBG (−8.6 to −8.0), FGBG (−8.2) and MGBG (−7.6) are higher than those of the Paleoproterozoic rocks (<−10; Li et al., 2007a), indicating that the mantle-derived components have been also involved in magma source. The Sr and Nd isotopic compositions of the CGBG and FGBG granites suggest that source materials are composed of two end-members, including ninety percent of Paleoproterozoic component with Nd model ages (T_{2DM}) of $(^{87}Sr/^{86}Sr)_i$ = 0.726589 and εNd(t) = −9.88 (Zhou, 2015), and ten percent of enriched mantle-derived component with $(^{87}Sr/^{86}Sr)_i$ and εNd(t) of 0.705420 and −1.9 (Li et al., 2004), respectively (Fig. 9a). Therefore, we can infer that the CGBG and FGBG are mainly derived from partial melting of the Paleoproterozoic basement with minor involvement of enriched mantle. A role for enriched mantle in the source has also been proposed for many other Mesozoic granites in South China, including the Bachi granite (zircon U-Pb age: 153.0 ± 1.0 Ma; Zhao et al., 2021), Fogang granites (zircon U-Pb age: ~160 Ma; Li et al., 2007a), Mantoushan granites (zircon U-Pb age: 163.8 ± 2.1 Ma; Zhang et al., 2015) and Xinfengjing granites (zircon U-Pb age: 160.6 ± 1.5 Ma; Zhang et al., 2015) all of which are associated with REE mineralization. Therefore, the enriched mantle has played an important role in the formation of the Mesozoic granites in South China. Meanwhile, the U-Th and Pb-Ce contents of the CGBG and FGBG suggest that the mantle source was metasomatized by melts from the subducted Paleo-Pacific oceanic slab and its sediments

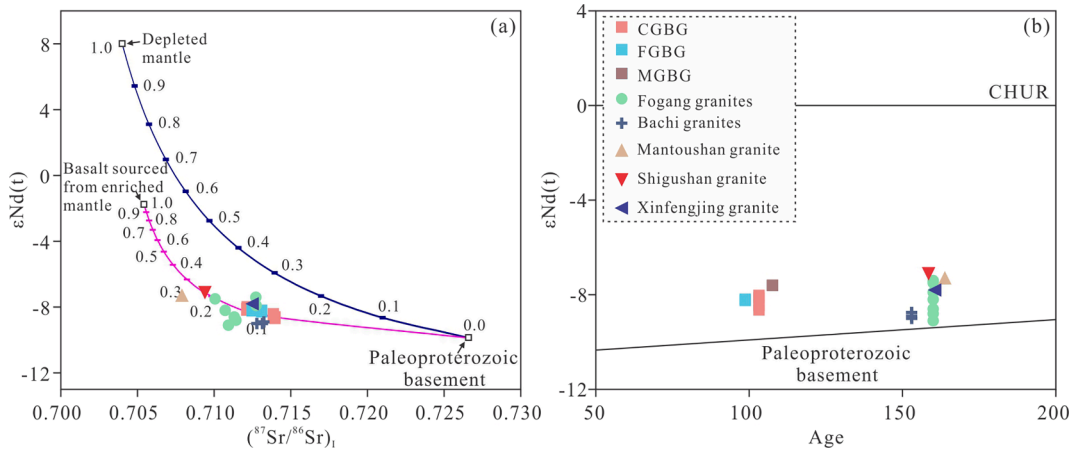

Fig. 9. Initial εNd(t) vs. $(^{87}Sr/^{86}Sr)_i$ of the CGBG, FGBG and MGBG granites (data of Fogang, Bachi, Mantoushan, Shigushan and Xinfengjing granites are from Li et al., 2007a, Zhang et al., 2015, Zheng, 2016; Zhao et al., 2021). The mixing model of two end-members: the data for depleted mantle-derived basaltic component ($^{87}Sr/^{86}Sr$ = 0.702, Sr = 200 ppm, εNd(t) = +8, Nd = 15 ppm) are from Wu et al. (2015), the enriched mantle basaltic component ($^{87}Sr/^{86}Sr$ = 0.70542, Sr = 772 ppm, εNd(t) = -1.9, Nd = 34.5 ppm) are from Li et al. (2004), and the Paleoproterozoic basement compositions are characterized by $^{87}Sr/^{86}Sr$ = 0.726589, Sr = 67.4 ppm, εNd(t) = -9.88 and Nd = 22.7 ppm according to Zhou, 2015.

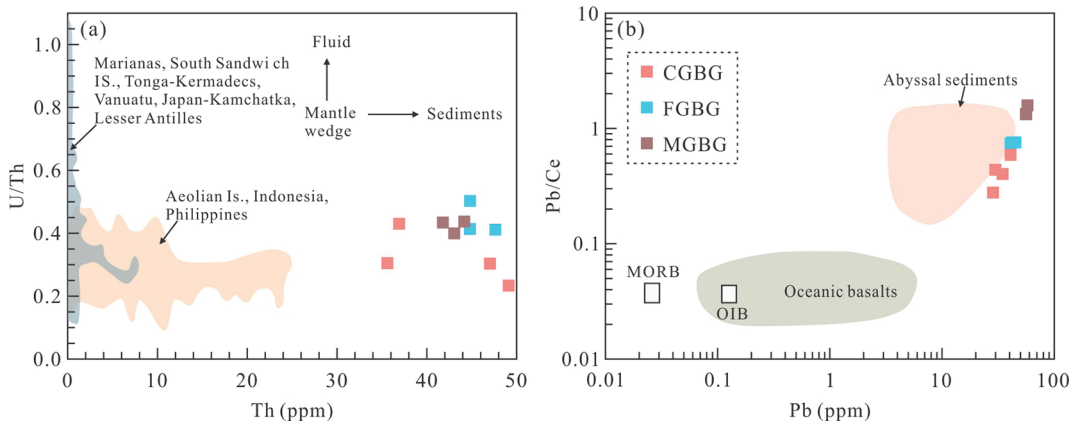

Fig. 10. Th vs. U/Th (a) and Pb vs. Pb/Ce (b) diagram for the CGBG, FGBG and MGBG.

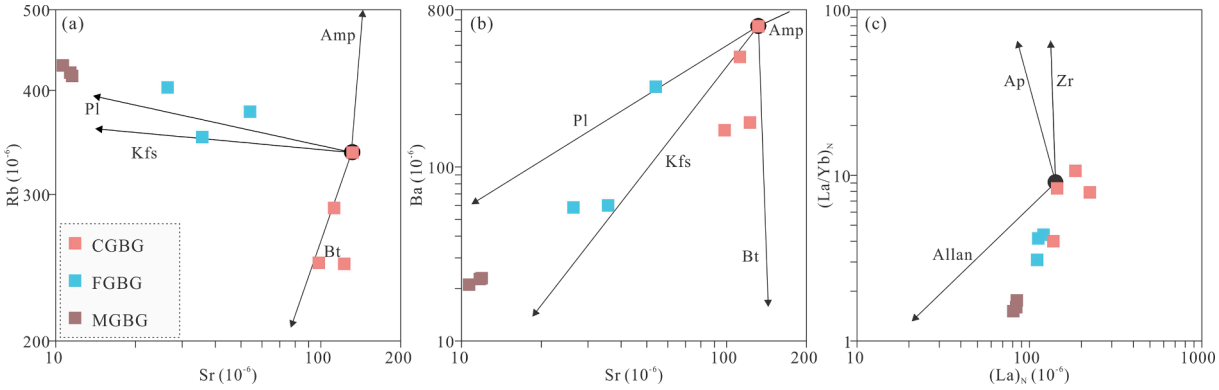

Fig. 11. Sr vs. Rb (a), Sr vs. Ba (b), and La_N vs. $(La/Yb)_N$ diagram for the CGBG, FGBG and MGBG showing fractionation crystallization of the main rock-forming minerals.

(Fig. 10; Othman et al., 1989; Hawkesworth et al., 1997). The MGBG has close space–time relations with the CGBG and FGBG, suggesting a possible genetic link. The MGBG has similar εNd(t) values as the CGBG, FGBG and many other late Mesozoic granitoids in South China (Mantoushan, Shigushan, Xinfengjing and Shilu; Fig. 9b), indicating that it was also likely sourced from partial melting of the major Paleoproterozoic rocks with minor involvement of an enriched mantle. The U-Th and Pb-Ce contents of the MGBG also suggest that the subduction-related melts from the subducted slab and its sediments have been involved in the enriched mantle (Fig. 10).

6.2. *Fractional crystallization process and implications for geodynamic settings*

At Gucheng, the CGBG, FGBG and MGBG have relatively high DI values (85.50–95.17) and SiO_2 contents (70.94–77.75 wt%), indicating that these three types of granites may have experienced intense fractional crystallization, which is also supported by the pronounced depletions of Ba, Sr, Rb, P, Ti and Eu. The depletion of Sr, Ba, Rb and Eu of CGBG, FGBG and MGBG is interpreted as fractionation of biotite, plagioclase or K-feldspar during the magmatic evolution (Fig. 11a-b). The depletion of Ti and P contents of the three types of granites indicates fractionation of Ti-bearing minerals (titanite and/or ilmenite) and

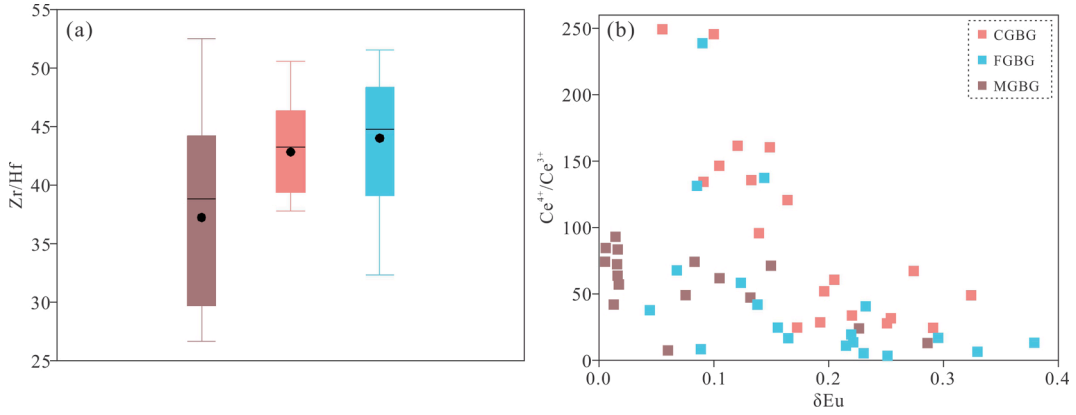

Fig. 12. Zircon Zr/Hf ratios (a), Ce^{4+}/Ce^{3+} vs. δEu diagram (b) and box plot of crystallization temperatures (c) of the CGBG, FGBG and MGBG granites.

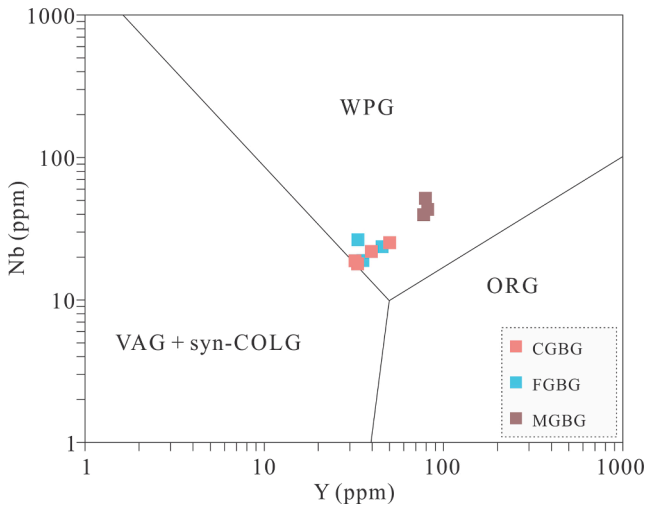

Fig. 13. Nb vs. Y diagram of Pearce et al. (1984) showing that the CGBG, FGBG and MGBG plotting in the field of within-plate granites (WPG).

apatite, respectively. Decreasing crystallization of allanite may account for the decreasing $(La/Yb)_N$ ratios from the CGBG through FGBG to MGBG (Fig. 11c).

Potassium (K) and Rb, Nb and Ta as well as Zr and Hf are considered to be "geochemical twins" because these three pairs of elements have the same charge and a similar ionic radium (Goldschmidt, 1937; Taylor and Mclennan, 1985). As a result, these three pairs of elements have similar geochemical properties and should not be fractionated during most geological processes (Goldschmidt, 1937; Taylor and Mclennan, 1985). It has been proposed that most magmatic rocks have K/Rb, Nb/Ta and Zr/Hf ratios of 195 to 433, 11 to 17.5, and 34.3 to 36.7, respectively (Shaw, 1968; Green, 1995; Münker et al., 2003; Rudnick and Gao, 2004). At Gucheng, the three types of granites have K/Rb, Nb/Ta and Zr/Hf ratios of 118 to 141, 5.3 to 13.4 and 30.9 to 34.3, 109 to 111, 5.0 to 6.0 and 23.5 to 25.9, and 88 to 90, 7.0 to 7.9 and 18.7 to 20.9, respectively, which have unusually low K/Rb, Nb/Ta and Zr/Hf ratios. Some authors have demonstrated that the K/Rb, Nb/Ta and Zr/Hf ratios would decrease in granites during fractional crystallization (Halliday et al., 1991; Raimbault et al., 1995; Chen and Yang, 2015; Ballouard et al., 2016). Therefore, the unusually low K/Rb, Nb/Ta and Zr/Hf ratios of these three types of granites may be due to intense fractional crystallization. It is noted that there is a decreasing trend of Zr/Hf and K/Rb ratios from the CGBG through the FGBG to the MGBG, indicating that MGBG is probably more evolved. Zr/Hf ratios in zircon is also one of the most reliable indicators of granitic magma evolution (Černý et al., 1985; Breiter et al., 2014). Previous studies have shown zircon from granitoids always contains some Hf and a general rule is that an increase in the Hf content coupled with a decrease in the Zr/Hf ratios in zircon is one of the most reliable indicators of granitic magma evolution (Černý et al., 1985; Breiter et al., 2014). At Gucheng, the MGBG zircons have lower Zr/Hf values (27–53, avg = 37) than those of CGBG (38–51, avg = 43) and FGBG (32–52, avg = 44) (Fig. 12a), also indicating that the barren MGBG is more evolved (Černý et al., 1985; Breiter et al., 2014).

On the other hand, previous studies have discovered that hydrothermal events could also decrease K/Rb and Zr/Hf ratios, and parameters of K/Rb < 150 (Shaw, 1968) and Zr/Hf < 26 (Bau, 1996) could distinguish granites affected by hydrothermal event after their crystallization. At Gucheng, the three types of granites all have K/Rb ratios lower than 150, and the FGBG and MGBG have Zr/Hf ratios lower than 26, indicating that the three types of granites all experienced hydrothermal events after their crystallization.

At Gucheng, the CGBG, FGBG and MGBG formed in the Late Cretaceous all have relatively high Nb and Y contents, and samples of these three types of rocks fall in the within-plate granite field (Fig. 13), also indicating that the three types of granites were formed in an extensional setting. This is consistent with that Cretaceous A-type granites (i.e., Ejinao, Dongpin and Naqin) occurred in the central and west part of the Guangdong Province, which are considered to be formed in an extensional setting associated with break-off of the Paleo-Pacific oceanic slab (Zhou, 2015).

6.3. *Implications for REE enrichment in granite and mineralization*

As discussed above, the enriched mantle metasomatized by melts associated with the subducted Paleo-Pacific oceanic slab was involved in magma source of CGBG, FGBG and MGBG as well as some other granites related to REE mineralization in South China (Fig. 8a). It has been suggested that the seafloor sediments contain significantly high REE abundance (up to 2200 ppm in the eastern Pacific Ocean; Kato et al., 2011), and melting of this sediment layer has a high potential for REE enrichment for the metasomatized mantle (Xu et al., 2017), and thus involvement of this enriched and metasomatized mantle in magma source of CGBG and FGBG at Gucheng has a great potential for REEs mineralization. Therefore, we can infer that the enriched mantle has played a primary role in REE mineralization, in which condition it can supply REE into magmas. On the other hand, the enriched mantle has also been involved in magma source of the MGBG, whilst it has no relation with REE mineralization, indicating that the REE mineralization has also been controlled by other factors.

As discussed above, crystallization of allanite occurred during formation of the CGBG, FGBG and MGBG (Fig. 11c). However, allanite is absent in the MGBG, and abundance of allanite of the FGBG is lower than those of the CGBG. Variation of abundance of allanite of these three types of granites is in contrast with degrees of magma evolution as discussed above, which is likely caused by crystal-melt segregation. Allanites were probably completely separated from magma associated with the most evolved MGBG (Romer and Siegesmund, 2003). Allanite is an important LREE-bearing mineral, and separation of allanite from magma could preferentially incorporate large volumes of LREE, resulting in relative depletion in LREE in the residual magma (Romer and Siegesmund, 2003). The abundance of crystallization and separation of allanite from melts is consistent with variations of LREE of the CGBG, FGBG and MGBG, also supporting this view (Fig. 7a).

Allanite is an important LREE-rich magmatic mineral in CGBG and FGBG, which suggests their great potential for LREE mineralization. The CGBG and FGBG associated with REE mineralization have DI values of 85.50–87.80 and 92.74–94.26, respectively, which is consistent with those of most LREE-enriched deposits (Li et al., 2017). Meanwhile, REE patterns of the CGBG and FGBG are characterized by enrichment of LREE, which is also consistent with granites associated with highly LREE-enriched deposit (Fogang; Bao and Zhao, 2003), but different from granites associated with highly HREE-enriched deposit (Zudong; Huang et al., 1989) (Fig. 7a). Li et al. (2017) have summarized that most of REE patterns of regolith are inherited from the parent rocks. These evidences all suggest that the Gucheng is very likely a LREE-enriched deposit, whilst HREE is more enriched in the regolith. Therefore, we can infer that despite of characteristics of the parent rocks, other factors can impose a significant control on the REE mineralization. As previous studies suggested, most of the granites associated with REE mineralization in South China were affected by a hydrothermal fluid after crystallization of granites (Li et al., 2017, 2019). At Gucheng, the CGBG and FGBG were also affected by a hydrothermal fluid, and the primary magmatic allanite and titanite grains in the CGBG and FGBG have been commonly replaced by hydrothermal fluid and altered into synchysite (LREE-rich) and gadolinite (HREE-rich), respectively (Fig. 4d-e). In these replacement processes, the hydrothermal fluid has transformed abundant LREE out of the allanite and HREE out of the titanite that have subsequently accommodated by synchysite and gadolinite, respectively. The LREE-rich synchysite and HREE-rich gadolinite are susceptible for chemical weathering (Li et al., 2017). Decompositions of synchysite and

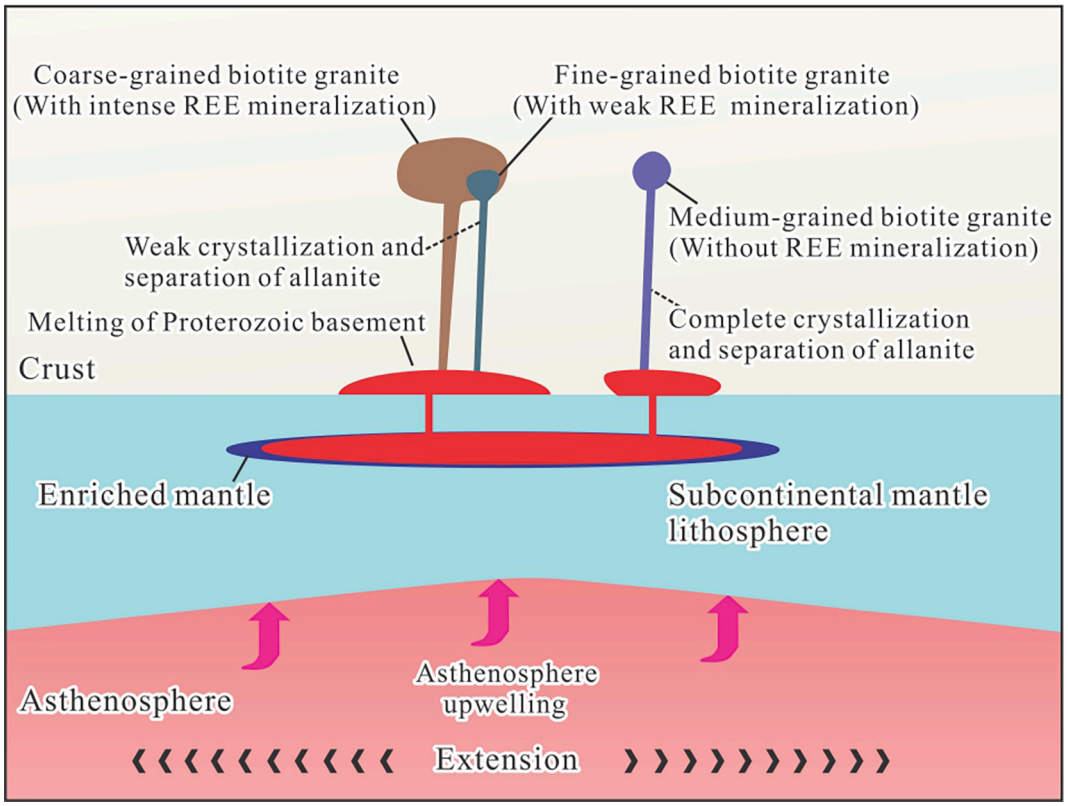

Fig. 14. A simple model showing magmatic evolution of the CGBG, FGBG and MGBG granites and associated REE mineralization.

gadolinite could contribute much of the LREE and HREE to the weathered crust, which is an important mechanism for both LREE and HREE mineralization at the Gucheng deposit as well as other regolith-hosted REE deposits in South China (Huang et al., 1989; Li et al., 2017).

Zircon is a common accessory mineral in igneous rocks and can incorporate REE in its lattice, of which Ce^{4+}/Ce^{3+} and Eu_N/Eu_N^* can be used to estimate magma oxidation state (Ballard et al., 2002; Dilles et al., 2015; Zhang et al., 2017). The measured zircon trace element concentrations and calculated Ce^{4+}/Ce^{3+} ratios and Eu_N/Eu_N^* of CGBG, FGBG and MGBG are listed in Supplementary Appendix 1. In our study, the CGBG and FGBG both have several Ce^{4+}/Ce^{3+} ratios (24.6 to 249.3 and 3.4 to 238.8) and Eu_N/Eu_N^* values (0.06 to 0.32 and 0.04 to 0.38) over 100 and 0.3, respectively (Fig. 12b), which is consistent with those of most porphyry Cu and Mo deposits (Shu et al., 2019). It has been proposed that porphyry Cu and Mo deposits are typically produced by oxidized magmas (Richards, 2003), and thus we can infer that the CGBG and FGBG granites were formed at a relative high oxygen environment. The MGBG have Ce^{4+}/Ce^{3+} ratios (7.4 to 93.0) and Eu_N/Eu_N^* values (0.01 to 0.29) <100 and 0.3, respectively, indicating that this type of granite was formed at a low oxygen environment, which is likely due to less involvement of enriched mantle in magma source than the CGBG and FGBG.

Above all, we can infer that an extensional environment may have caused asthenosphere upwelling in South China in the Late Mesozoic (Li et al., 2007b). The melts with abundant REE (produced by partial melting of an enriched lithosphere mantle metasomatized by subduction-related melts) ascent into the lower continental crust, inducing partial melting of the lower crust (Paleoproterozoic basement). This melt with abundant REE has experienced complete crystallization and separation of allanite during its ascending, forming the barren MGBG without significant REE enrichment. Intrusions of the CGBG and FGBG are closely associated with REE mineralization occurred subsequently during continuous extension, with higher oxygen fugacity induced by more involvement of enriched mantle (Fig. 14). This melt also with abundant REE has experienced relatively low crystallization and separation of allanite due to its less evolution, and abundant allanite remain in the melt, resulting in relative enrichment of LREE in the CGBG and FGBG. The hydrothermal event together with the replacement of magmatic allanite and titanite for the enrichment of both LREE and HREE reported in this study may play a more important role for REE mineralization at Gucheng.

7. Conclusions

(1) At Gucheng, the CGBG, FGBG and MGBG were all formed in the Late Cretaceous. These three types of granites are all formed in an extensional setting.
(2) The CGBG, FGBG and MGBG are all I-type granites, but the FGBG and MGBG are more fractionated and less evolved.
(3) Involvement of enriched mantle, crystallization and separation of allanite as well as involvement of a hydrothermal fluid during the latest stage of magmatic crystallization are important factors controlling REE mineralization at Gucheng.

Declaration of Competing Interest

The authors declare that they have no known competing financial interests or personal relationships that could have appeared to influence the work reported in this paper.

Data availability

Data will be made available on request.

Acknowledgements

This study was funded by the Guangdong Major Project of Basic and Applied Basic Research (No. 2019B030302013), the National Natural

Science Foundation of China, China (No. 42103058, 41725009, 41921003, 42173065), Special Research Assistant Project, Director's Fund of Guangzhou Institute of Geochemistry, CAS and Science and Technology Planning of Guangdong Province, China (2020B1212060055). Staff of the Key Geology Bureau for Nonferrous Metals of Guangdong Province are thanked for supporting the research and for providing access to drill cores and sample collection. Pete. Hollings is thanked for his comments on an early version of this paper.

Appendix A. Supplementary data

Supplementary data to this article can be found online at https://doi.org/10.1016/j.oregeorev.2022.105034.

References

Asadi, S., Moore, F., Zarasvandi, A., 2014. Discriminating productive and barren porphyry copper deposits in the southeastern part of the central Iranian volcano-plutonic belt, Kerman region, Iran: a review. Earth-Sci. Rev. 138, 25–46.
Ballard, J.R., Palin, J.M., Campbell, I.H., 2002. Relative oxidation states of magmas inferred from Ce (IV)/Ce(III) in zircon: application to porphyry copper deposits of northern Chile. Contrib Mineral Petrol. 144, 347–364.
Ballouard, C., Poujol, M., Boulvais, P., Branquet, Y., Tartèse, R., Vigneresse, J.L., 2016. Nb-Ta fractionation in peraluminous granites: A marker of the magmatic-hydrothermal transition. Geology 44, 231–234.
Bao, Z.W., Zhao, Z.H., 2003. Geochemistry and tectonic setting of the Fogang aluminous A-type granite, Guangdong Province, China–a preliminary study. Geol. Geochem. 31, 52–61 in Chinese with English abstract.
Bau, M., 1996. Controls on the fractionation of isovalent trace elements in magmatic and aqueous systems: Evidence from Y/Ho, Zr/Hf, and lanthanide tetrad effect. Contrib. Mineral. Petrol. 123, 323–333.
Breiter, K., Lamarão, C.N., Borges, R.M.K., Dall'Agnol, R.,, 2014. Chemical characteristics of zircon from A-type granites and comparison to zircon of S-type granites. Lithos. 192–195, 208–225.
Černý, P., Meintzer, R.E., Anderson, A.J., 1985. Extreme fractionation in rare-element granitic pegmatites: selected examples of data and mechanisms. Canadian Mineral. 23, 381–421.
Chappell, B.W., White, A.J.R., Wyborn, D., 1987. The importance of residual Source material (restite) in granite petrogenesis. J. Petrol. 28, 1111–1138.
Chappell, B.W., 1999. Aluminium saturation in I- and S-type granites and the characterization of fractionated haplogranites. Lithos. 46, 535–551.
Chen, J.F., Guo, X.S., Tang, J.F., Zhou, T.X., 1999. Nd isotopic model ages: implications of the growth of the continental crust of southeastern China. J. Nanjing Univ. (Natural sciences). 35 (6), 649–658 in Chinese with English abstract.
Chen, J.Y., Yang, J.H., 2015. Petrogenesis of the Fogang highly fractionated I-type granitoids: Constraints from Nb, Ta, Zr and Hf. Acta Petrol. Sin. 31 (3), 846–854 in Chinese with English abstract.
Clemens, J.D., Stevens, G., Farina, F., 2011. The enigmatic sources of I-type granites: The peritectic connexion. Lithos 126 (3–4), 174–181.
Dilles, J.H., Kent, A.J.R., Wooden, J.L., Tosdal, R.M., Koleszar, A., Lee, R.G., Farmer, L.P., 2015. Zircon compositional evidence for sulfur-degassing from ore-forming arc magmas. Econ Geol. 110, 241–251.
Goldschmidt, V.M., 1937. The principles of distribution of chemical elements in minerals and rocks: The seventh Hugo Müller Lecture delivered before the Chemical Society on March 17th, 1937. J. Chem. Soc. 655–673.
Green, T.H., 1995. Significance of Nb/Ta as an indicator of geochemical processes in the crust-mantle system. Chem. Geol. 120, 347–359.
Halliday, A.N., Davidson, J.P., Hildreth, W., Holden, P., 1991. Modelling the petrogenesis of high Rb/Sr silicic magmas. Chem. Geol. 92, 107–114.
Hawkesworth, C.J., Turner, S.P., McDermott, F., Peate, D.W., van Calsteren, P., 1997. U-Th isotopes in arc magmas: implications for element transfer from subducted crust. Science 276, 551–555.
Hawkesworth, C.J., Kemp, A.I.S., 2006. Using hafnium and oxygen isotopes in zircons to unravel the record of crustal evolution. Chem. Geol. 226, 144–162.
Huang, D., Wu, C., Han, J., 1989. REE geochemistry and mineralization characteristics of the Zudong and Guanxi granites, Jiangxi Province. Acta Geol. Sin. 2, 139–157.
Irvine, T.H., Baragar, W.R.A., 1971. A guide to the chemical classification of the common volcanic rocks. Canadian J. Earth Sci. 8, 523–548.
Jahn, B.M., Wu, F.Y., Chen, B., 2000. Massive granitoid generation in Central Asia: Nd isotope evidence and implication for continental growth in the Phanerozoic. Episodes 23, 82–92.
Jowitt, S., Wong, V., Wilson, S., Gore, O., 2017. Critical metals in the critical zone: controls, resources and future prospectivity of regolith-hosted rare earth elements. Aust. J. Earth Sci. 64, 1045–1054.
Kato, Y., Fujinaga, K., Nakamura, K., Takaya, Y., Kitamura, K., Ohta, J., Toda, R., Nakashima, T., Iwamori, H., 2011. Deep-sea mud in the Pacific Ocean as a potential resource for rare-earth elements. Nat. Geosci. 4, 535–539.
Kemp, A.I.S., Hawkesworth, C.J., Paterson, B.A., Kinny, P.D., 2006. Episodic growth of the Gondwana supercontinent from hafnium and oxygen isotopes in zircon. Nature 439, 580–583.
Kemp, A.I.S., Hawkesworth, C.J., Foster, G.L., Paterson, B.A., Woodhead, J.D., Hergt, J. M., Gray, C.M., Whitehouse, M.J., 2007. Magmatic and crustal differentiation history of granitic rocks from Hf-O isotopes in zircon. Science 315, 980–983.
Koschek, G., 1993. Origin and significance of the SEM cathodoluminescence from zircon. J. Microsc. 171, 223–232.
Li, M.Y.H., Zhao, W.W., Zhou, M.F., 2017. Nature of parent rocks, mineralization styles and ore genesis of regolith-hosted REE deposits in South China: An integrated genetic model. J. Asian Earth Sci. 148, 65–95.
Li, M.Y.H., Zhou, M.F., Williams-Jones, A.E., 2019. The Genesis of Regolith-Hosted Heavy Rare Earth Element Deposits: Insights from the World-Class Zudong Deposit in Jiangxi Province, South China. Econ. Geol. 2019, 114(3), 541–568.
Li, M.Y.H., Zhou, M.F., 2020. The role of clay minerals in formation of the regolith-hosted heavy rare earth element deposits. Am. Mineral. 105, 92–108.
Li, X.H., Chung, S.L., Zhou, H.W., Lo, C.H., Liu, Y., Chen, C.H., 2004. Jurassic intraplate magmatism in southern Hunan-eastern Guangxi: 40Ar/39Ar dating, geochemistry, Sr-Nd isotopes and implications for the tectonic evolution of SE China. Geol., Lond., Spec. Publ. 226, 193–215.
Li, X.H., Li, Z.X., Li, W.X., Liu, Y., Yuan, C., Wei, G.J., Qi, C.S., 2007. U-Pb zircon, geochemical and Sr-Nd-Hf isotopic constraints on age and origin of Jurassic I- and A-type granites from central Guangdong, SE China: A major igneous event in response to foundering of a subducted flat-slab? Lithos 96, 186–204.
Liu, Y.S., Hu, Z.C., Gao, S., Günther, D., Xu, J., Gao, C.G., Chen, H.H., 2008. In situ analysis of major and trace elements of anhydrous minerals by LA-ICP-MS without applying an internalstandard. Chem. Geol. 257, 34–43.
Maniar, P.D., Piccoli, P.M., 1989. Tectonic discrimination of granitoids. Geol. Soc. Am. Bull. 101 (5), 635–643.
Murakami, H., Ishihara, S., 2008. REE mineralization of weathered crust and clsy sediment on granitic rocks in the Sanyo Belt, SW Japan and the Southern Jiangxi Province. China. Resour. Geol. 58, 373–401.
Münker, C., Pfander, J.A., Weyer, S., Buchl, A., Kleine, T., Mezger, K., 2003. Evolution of planetary cores and the earth-moon system from Nb/Ta systematics. Science 301 (5629), 84–87.
Othman, D.B., White, W.M., Patchett, J., 1989. Geochemistry of marine sediments, island arc magma genesis and crust–mantle recycling. Earth Planet. Sci. Lett. 94, 1–21.
Pearce, J.A., Harris, N.B.W., Tindle, A.G., 1984. Trace element discrimination diagrams for the tectonic interpretation of granitic rocks. J. Petrol. 25, 956–983.
Peccerillo, A., Taylor, A.R., 1976. Geochemistry of Eocene calc-alkaline volcanic rocks from the Kastamonu area, Northern Turkey. Contrib. Mineral. Petrol. 58 (1), 63–81.
Raimbault, L., Cuney, M., Azencott, C., Duthou, J.L., Joron, J.L., 1995. Geochemical evidence for a multistage magmatic genesis of Ta-Sn-Li mineralization in the granite at Beauvoir, French Massif Central. Econ. Geol. 90, 548–576.
Reed, W.P., 1992. Certificate of Analysis: Standard Reference Materials 610 and 611. National Institute of Standards and Technology.
Richards, J.P., 2003. Tectono-magmatic precursors for porphyry Cu-(Mo-Au) deposit formation. Econ. Geol. 98, 1515–1533.
Romer, R.L., Siegesmund, S., 2003. Why allanite may swindle about its true age. Contrib. Mineral Petrol. 146, 297–307.
Rudnick, R.L., Gao, S., 2004. Compositions of the continental crust. In: Holland, H.D., Turekian, K.K. (Eds.), Treatise on Geochemistry, 3. Elsevier, Amsterdam, pp. 1–64.
Sanematsu, K., Watanabe, Y., 2016. Characteristics and genesis of ion-adsorption type deposits. Rev. Econ. Geol. 18, 55–79.
Shaw, D., 1968. A review of K-Rb fractionation trends by covariance analysis. Geochim. Cosmochim. Acta 32, 573–601.
Shu, Q.H., Chang, Z.S., Lai, Y., Hu, X.L., Wu, H.Y., Zhang, Y., Wang, P., Zhai, D.G., Zhang, C., 2019. Zircon trace elements and magma fertility: insights from porphyry (-skarn) Mo deposits in NE China. Miner. Depos. 54 (5), 645–656.
Singer, B.S., Myers, J.D., Frost, C.D., 1992. Mid-Pleistocene lavas from the Seguam volcanic center, central Aleutian arc: closed-system fractional crystallization of a basalt to rhyodacite eruptive suite. Contrib. Mineral. Petrol. 110 (1), 87–112.
Soesoo, A., 2000. Fractional crystallization of mantle-derived melts as a mechanism for some I-type granite petrogenesis: an example from Lachlan Fold Belt, Australia. J. Geol. Soc. 135–149.
Streckeisen, A., Le Maitre, R.W., 1979. A chemical approximation to the modal QAPF classification of the igneous rocks. Neues Jahrb. Mineral. Abh. 136, 169–203.
Sun, S.S., McDonough, W.F., 1989. Chemical and isotopic systematics of oceanic basalt: implications for mantle composition and processes. In: Saunders, A.D., Norry, M.J. (Eds.), Magmatism in the Ocean Basins. Geol. Soc. Spec. Publ., vol. 42, pp. 528–548.
Taylor, S.R., McLennan, S.M., 1985. The continental Crust: Its composition and Evolution. Blackwell Scientific, Oxford, p. 312.
Whalen, J.B., Jenner, G.A., Longstaffe, F.J., 1996. Geochemical and isotopic (O, Nd, Pb and Sr) constraints on A-type granite petrogenesis based on the Topsails Igneous Suite, Newfoundland Appalachians. J Petrol. 87, 1463–1489.
Wiedenbeck, M., Allé, P., Corfu, F., Griffin, W.L., Meier, M., Oberli, F., Von Quadt, A., Roddick, J.C., Spiegel, W., 1995. Three natural zircon standards for U-Th-Pb, Lu-Hf, trace element and REE analyses. Geostandards Newslett. 19 (1), 1–23.
Wolf, M.B., London, D., 1994. Apatite dissolution into peraluminous haplogranite melts: An experimental study of solubilities and mechanisms. Geochim. Cosmochim. Acta 58, 4127–4145.
Wu, C., Chen, H.Y., Hollings, P., Xu, D.R., Liang, P., Han, J.S., Xiao, B., Cai, K.D., Liu, Z. J., Qi, Y.K., 2015. Magmatic sequences in the Halasu Cu Belt, NW China: Trigger for the Paleozoic porphyry Cu mineralization in the Chinese Altay-East Junggar. Ore Geol. Rev. 71, 373–404.
Xie, Y.L., Hou, Z.Q., Goldfarb, R.J., Guo, X., Wang, L., 2016. Rare earth element deposits in China. Rev. Econ. Geol. 18, 115–136.

Xu, C., Kynicky, J., Smith, M.P., Kopriva, A., Brtnicky, M., Urubek, T., Yang, Y.H., Zhao, Z., He, C., Song, W.L., 2017. Origin of heavy rare earth mineralization in South China. Nat. Commun. 8, 14598.
Zhang, C.C., Sun, W.D., Wang, J.T., Zhang, L.P., Sun, S.J., Wu, K., 2017. Oxygen fugacity and porphyry mineralization: a zircon perspective of Dexing porphyry Cu deposit, China. Geochim. Cosmochim. Acta 206, 343–363.
Zhang, W., Hu, Z.C., 2020. Estimation of isotopic reference values for pure materials and geological reference materials. At. Spectrosc. 41 (3), 93–102.
Zhang, Y., Cheng, J.M., Tian, J., Pan, J., Sun, S.Q., Zhang, L.J., Zhang, S.T., Chu, G.B., Zhao, Y.J., Lai, C., 2019. Texture and trace element geochemistry of quartz in skarn system: Perspective from Jiguanzui Cu-Au skarn deposit, Eastern China. Ore Geol. Rev. 109, 535–544.
Zhang, Y., Yang, J.H., Sun, J.F., Zhang, J.H., Chen, Y.J., Li, X.H., 2015. Petrogenesis of Jurassic fractionated I-type granites in Southeast China: Constraints from whole-rock geochemical and zircon U-Pb and Hf-O isotopes. J. Asian Earth Sci. 111, 268–283.
Zhao, W.W., Zhou, M.F., Li, M.Y.H., Zhao, Z., Gao, J.F., 2017. Genetic types, mineralization styles and geodynamic settings of Mesozoic tungsten deposits in South China. J. Asian Earth Sci. 137, 109–140.
Zhao, X., Li, N.B., Huizenga, J.M., Yan, S., Yang, Y.Y., Niu, H.C., 2021. Rare earth element enrichment in the ion-adsorption deposits associated granites at Mesozoic extensional tectonic setting in South Chin. Ore Geol. Rev. 137, 104317.
Zheng, W., 2016. The Yanshanian minerogenetic series and mineralization of polymetallic deposit in the Yangchun Basin of Yunkai area, South China. China University of Geosciences, Beijing 50–146 in Chinese with English abstract.
Zhou, Z.M., 2015. Late Mesozoic Polycyclic Tectono-Magmatic Evolution and Forming Mechanism of the Geothermal Systems in South China-New Constraints from Typical Plutons in Guangdong Province. China University of Geosciences, Wuhan 1–85 in Chinese with English abstract.